Global and Planetary Change 242 (2024) 104585

Contents lists available at ScienceDirect

Global and Planetary Change

journal homepage: www.elsevier.com/locate/gloplacha

The expression of the MIS 12 glacial stage in Southeastern Europe and its impact over the Middle Pleistocene hominins in Megalopolis Basin (Greece)

Geanina A. Butiseacă [a,*], Iuliana Vasiliev [b], Marcel T.J. van der Meer [c], Ines J.E. Bludau [d,e], Panagiotis Karkanas [f], Vangelis Tourloukis [a,g], Annett Junginger [d,e], Andreas Mulch [b,h], Eleni Panagopoulou [i], Katerina Harvati [a,d,j]

[a] Eberhard Karls Universität Tübingen, Department of Geosciences, Institute of Archaeological Sciences, Palaeoanthropology, Tübingen, Germany
[b] Senckenberg Biodiversity and Climate Research Centre, Frankfurt am Main, Germany
[c] NIOZ Royal Netherlands Institute for Sea Research, Department of Marine Microbiology and Biogeochemistry, Den Burg, Texel, the Netherlands
[d] Senckenberg Centre for Human Evolution and Palaeoenvironment, Tübingen, Germany
[e] Eberhard Karls Universität Tübingen, Department of Geosciences, Micropalaeontology, Tübingen, Germany
[f] M. H. Wiener Laboratory for Archaeological Science, American School of Classical Studies at Athens, Athens, Greece
[g] Department of History and Archaeology, University of Ioannina, Ioannina, Greece
[h] Goethe University Frankfurt, Institute of Geosciences, Frankfurt am Main, Germany
[i] Ephorate of Palaeoanthropology-Speleology, Hellenic Ministry of Culture, Athens, Greece
[j] DFG Centre for Advanced Studies 'Words, Bones, Genes, Tools: Tracking Linguistic, Cultural and Biological Trajectories of the Human Past, Tübingen, Germany

ARTICLE INFO

Editor: Dr. Fabienne Marret-Davies

Keywords:
Pleistocene
Lower Palaeolithic
Palaeoclimate
SE Europe
Organic geochemistry
Stable isotopes
Glacial refugia

ABSTRACT

Southern Europe is hypothesized to have acted as a glacial refugium for hominin populations during the Pleistocene. Of particular importance is South-East Europe, which most likely played a dual role, both as refugium and dispersal corridor, especially during the Middle Pleistocene glaciations, when drastic climatic conditions led to major sea level drops in the Aegean. However, little is known about the palaeoenvironmental conditions at the time of hominin presence in this region, making these hypotheses difficult to test. Here we analyze biomarker data and leaf wax stable isotopic compositions of the MIS 12 Lower Palaeolithic site Marathousa 1 (Megalopolis Basin, Greece) to assess the climatic conditions accompanying the time of hominin presence in the area. Our data indicate a major cooling affecting the north Mediterranean/Aegean domain during this time interval, with lowest temperatures recorded between ~440–432 ka. The glacial peak is associated with changes in vegetation (i.e., from more forested to more open landscape), reduction of humidity and water availability (i.e., moisture depletion, increased evaporation). Hominins are present at the Marathousa 1 location at the end of this interval (434–432 ka), confirming that the Megalopolis Basin served as a refugium for hunter-gatherer groups during periods of harsh climatic conditions. Additionally, the progressive cooling is associated with an important sedimentary hiatus between ~465–440 ka reflected in all circum-Mediterranean records (both marine and continental), indicating a regional impact of the MIS 12 glaciation over surface processes.

1. Introduction

Marine Isotope Stage 12 (MIS 12; 478–424 ka) represents one of the strongest Quaternary/Pleistocene glaciations, characterized by a maximum expansion of continental ice sheets in the Northern Hemisphere (Lisiecki and Raymo, 2005; Koutsodendris et al., 2019). Most available information on MIS 12 in the Mediterranean area predominantly derives from marine records (e.g., Müller et al., 1998; Martínez-Dios et al., 2021), while its impact on the southern European terrestrial palaeoclimate and palaeoecosystems remains poorly constrained, limiting the knowledge of its influence on the hominins in the region. Knowledge on the palaeoclimatic conditions of specific archaeological sites is particularly important for archaeological research, because of the highly fluctuating Quaternary climate. Due to the typically spatially and temporally restricted hominin fossil occurrence, such studies need to be embedded in longer stratigraphic and palaeoclimatic time series.

The Marathousa 1 (MAR-1) is an open section of ~6.5 m thickness, on the margin of Megalopolis open cast mine, located in the Megalopolis

* Corresponding author.
E-mail address: geanina-adriana.butiseaca@ifu.uni-tuebingen.de (G.A. Butiseacă).

https://doi.org/10.1016/j.gloplacha.2024.104585
Received 15 July 2024; Received in revised form 4 September 2024; Accepted 13 September 2024
Available online 15 September 2024

Basin, Peloponnese, Greece (Panagopoulou et al., 2018). Its excavation from 2013 to 2019 has yielded a rich record of human activity, including an extensive lithic assemblage (Tourloukis et al., 2018a; Guibert-Cardin et al., 2022) associated with both faunal and botanical remains (e.g., Doukas et al., 2018; Field et al., 2018; Konidaris et al., 2018, 2022; Michailidis et al., 2018; Blackwell et al., 2018; Roditi et al., 2024), suggesting that the region provided shelter for various biotic groups, probably as a result of the continuous presence of fresh water sources (Bludau et al., 2021).

Here we show that the hominin presence at the site is associated with the end of the MIS 12 glacial maximum, providing a direct link between climate (i.e., cold periods) and the presence of human populations in the basin. We have reconstructed mean annual air temperature (MAAT) and mean annual temperature above freezing (MAF) based on branched glycerol dialkyl glycerol tetraethers (brGDGTs), biomarkers produced by soil, lacustrine and riverine bacteria. Additionally, we provide compound-specific hydrogen (δ^2H) and carbon ($\delta^{13}C$) isotope data from mid and long chain *n*-alkanes (produced by aquatic and higher terrestrial plants, respectively) to monitor changes in moisture and vegetation response in the catchment of the Marathousa 1 site. Furthermore, the *n*-alkane-based ratios (such as carbon preference index (CPI), average chain length (ACL), aquatic plant index (P_{aq}) and grass/tree ratio (C_{31}/C_{27}) are used to complete a comprehensive understanding of changes recorded in both terrestrial and aquatic domains in Marathousa 1 starting with the end of MIS 13, during the preserved MIS 12 glacial stage, and the onset of MIS 11. We substantiate these data by earlier acquired microfauna and inorganic geochemistry records from Marathousa 1 (Bludau et al., 2021) and further compare our results with the existing time equivalent records from the Balkans (Koutsodendris et al., 2019) and Mediterranean regions (Ardenghi et al., 2019; Martínez-Dios et al., 2021; Regattieri et al., 2016).

The brGDGTs, plant waxes and their δ^2H and $\delta^{13}C$ data produced in this contribution provide a first quantification of the changes in the environmental conditions, as well as vegetation response to hydrology and temperature fluctuations, providing the base for evaluating the potential impact of climatic and environmental changes on human populations as recorded in the Lower Palaeolithic site Marathousa 1.

2. Geological and archaeological setting

Marathousa 1 is located in the Megalopolis Basin (Greece; Fig. 1), inside the open-cast lignite mine of Megalopolis, where mining activities over the past several decades have exposed thick sequences of fossiliferous deposits (e.g., Panagopoulou et al., 2018; Harvati et al., 2018 and references therein). The basin is an extensional structure with NNE – SSW direction during the Pliocene (Vinken, 1965) and NE – SW during Pleistocene (Karkanas et al., 2018), with the sedimentary filling accommodated by the fault system activity.

Marathousa 1 comprises two areas of investigation, Area A and Area B, located within 60 m of one another. Area B, the focus of this study, has a longer stratigraphical record, with ten defined sedimentary units (UB1 – UB10). The entire sequence is part of the Middle Pleistocene fluvio-lacustrine deposits of the Marathousa member (Tourloukis et al., 2018b), with silts and sands as dominant lithology (Karkanas et al., 2018).

The archaeological horizon occurs in the middle part of a clastic sequence that is sandwiched between the base of lignite seam IIIa (UB1, top profile) and lignite seam IIb (UB10, base profile; Karkanas et al., 2018). Based on the palaeontological findings, Marathousa 1 is considered a butchering site, representing the only Lower Palaeolithic locality with exploitation of proboscideans reported in Southeastern Europe. It also preserves ungulates, small mammals, birds and reptiles (Konidaris et al., 2018, 2022; Doukas et al., 2018; Michailidis et al., 2018; Field et al., 2018). In Area B, the main artifact-bearing interval is found at a local erosional contact between units UB4c and UB5a, but artifacts occur inside the two units as well (in unit UB5a - directly underlying the contact, while in UB4b - directly above the contact). For a detailed discussion of the exposed palaeosurface represented by the UB5a-UB4c contact and the related site formation processes see Karkanas et al. (2018) and Giusti et al. (2018). We consider Area B more suitable for palaeoenvironmental analyses due to its more complete stratigraphic coverage than area A.

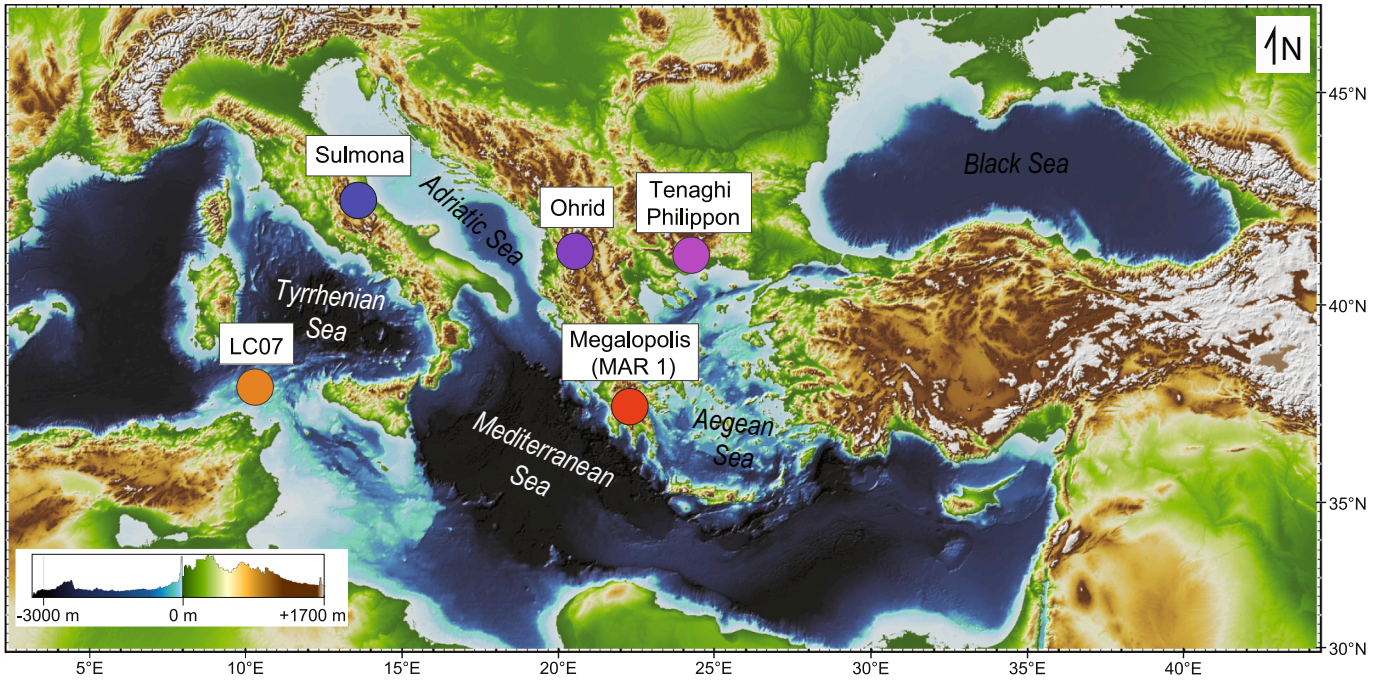

Fig. 1. Map showing the location of Marathousa 1 site and existing continental sites with MIS 12 sedimentary records. The colour scale on the left side shows the elevation. Map modified after Bludau et al. (2021).

3. Present-day climate parameters

Current climate in Greece is predominantly Mediterranean, with hot and dry summers, mild winters (Kutzbach et al., 2014) and strongly seasonal precipitations distribution (~750–1000 mm/year; Okuda et al., 2002). Most precipitations occur during winter (December–January) due to storm tracks generated by the convergence of the warm Mediterranean air masses with North Atlantic and Eurasian cold air influxes (Kutzbach et al., 2014).

The Peloponnese peninsula is characterized by a true Mediterranean climate (Köppen, 1918) due to its geographical position and is slightly warmer and dryer than the rest of continental Greece. According to the Hellenic National Meteorological Service (HNMS), the Megalopolis basin receives ~815 mm/year precipitations and benefits from long sun exposure (~ 2670 h/year). The measured mean air annual temperature between 1971 and 2000 was 15.8 °C, with a mean low of 9.4 °C and a mean high of 20.6 °C. The lowest registered temperature was ~3 °C in January–February, while the maximum of ~31 °C in July–August (HNMS Climatic Atlas 1971–2000; http://climatlas.hnms.gr/sdi/).

The main drivers for the short and mid-term precipitation and temperature variabilities in the Mediterranean area are large-scale circulation patterns such as the North Atlantic Oscillation (NAO) and the Atlantic Multidecadal Oscillation (AMO), controlling the intensity and extension of storm tracks (Mann et al., 2009; Kutzbach et al., 2014; Lüning et al., 2019). Strong storm tracks are associated with negative phases of NAO and AMO, while droughts are associated with positive phases (Kutzbach et al., 2014; Lüning et al., 2019). The long-term climate though is influenced by orbital parameters (Laskar et al.,

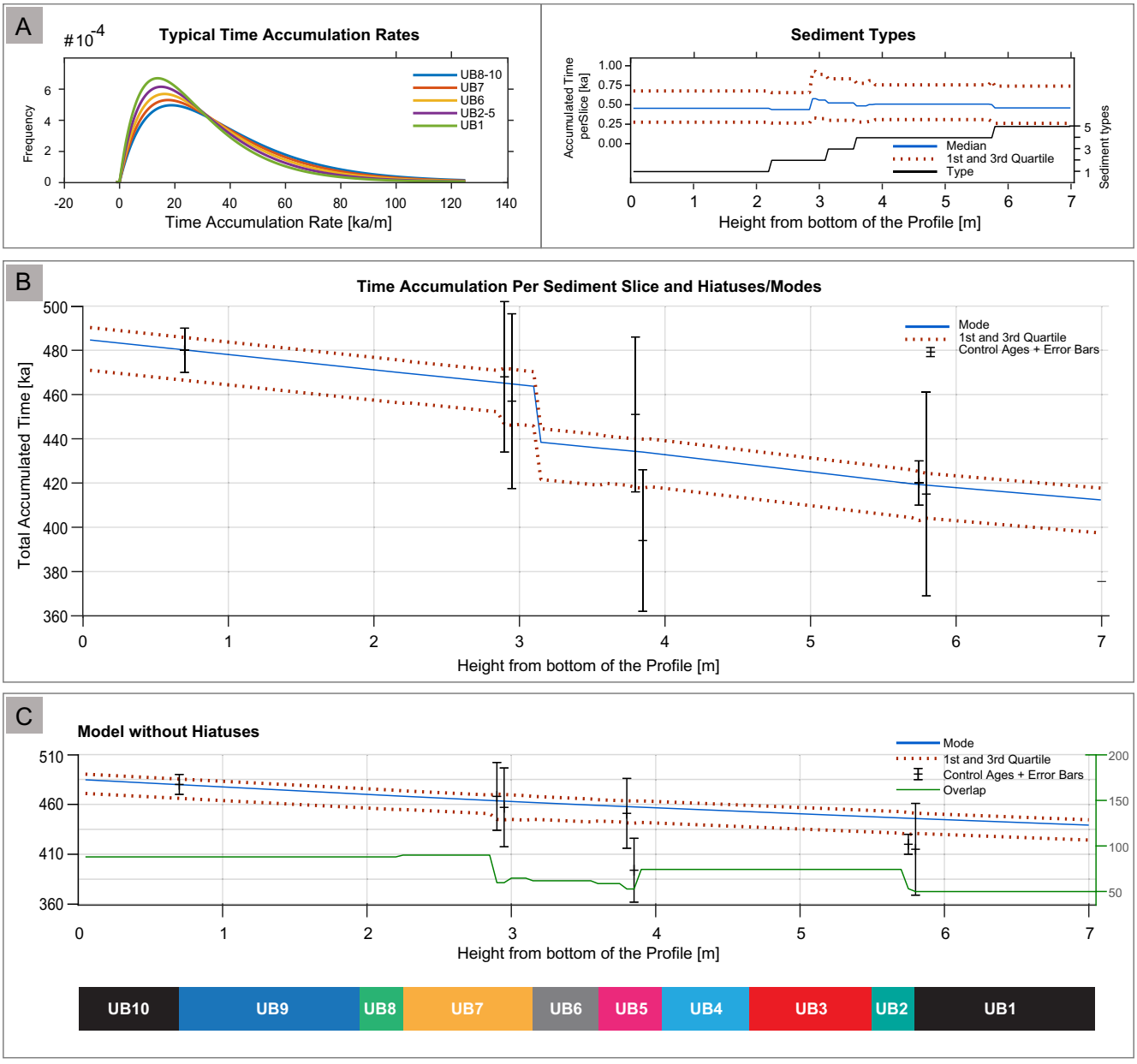

Fig. 2. Revised Marathousa 1 age model. A panel (upper left): Resulting gamma distribution curves of the different sediment units based on input sediment parameters (shape and scale factor). Green: UB8 – UB10 (shape 2, scale 7.5). Orange: UB7 (2, 7). Yellow: UB6 (2, 6.5). Violet: UB2 – UB5 (2, 6). Green: UB1 (2, 5.5). U: Distribution of the sediment units (black) and median accumulated time per sediment slice (blue and dotted red lines). B: Mode of final merged age model with hiatus (blue), error margins (dotted red), datings and their error bars (black). C: Preliminary age model (blue) without hiatus, error margins (dotted red), datings and their error bars (black). Percentage of overlap of the two initial preliminary models (green). Below are represented the sedimentary units. (For interpretation of the references to colour in this figure legend, the reader is referred to the web version of this article.)

2004), especially obliquity and precession (Kroon et al., 1998; Lourens, 2004), which are controlling the glacial-interglacial phases, as well as major changes in vegetation (Joannin et al., 2011) and precipitation patterns.

4. Materials and methods

4.1. Revised site chronology

Bludau et al. (2021) created a Bayesian age model for the MAR-1 sequence based on its chronostratigraphic attribution to MIS 12 (Tourloukis et al., 2018b), as well as on optically stimulated luminescence (OSL) dates produced by the pMET-pIRIR dating method (Jacobs et al., 2018). The initial age model of Bludau et al. (2021) did not account for a major hiatus present in the middle part of the MAR-1 sequence, (UB6; Karkanas et al., 2018). Considering subsequent observations hinting at a hiatus between UB7 and UB6, a new age model is developed here (Fig. 2; Supplementary table 1) using a modified age modelling approach originally presented by Trauth (2014). Importantly, no significant hiatus was detected at the archaeological site, between UB5 and UB4 (Karkanas et al., 2018; Giusti et al., 2018). The model utilizes the MATLAB software, which takes hiatuses into account. The temporal tie points of the sequence are 480 and 420 ka (±10 ka error) respectively, like those used by Bludau et al. (2021). Also, similar input parameters were applied, reflecting the depositional properties of the sedimentary units (Supplementary table 2). The code computes two different preliminary models. The first is based on the input sediment parameters and the second, statistically independent, is based on the input ages. Both models are considered equally valid. In the final model the preliminary ones are merged. This newly computed age model places the MAR-1 sequence between 485 and 412 ka and hence incorporating the preserved sedimentary record of the glacial stage of MIS 12.

4.2. Organic geochemistry

4.2.1. Lipid extraction and analysis

Thirty-six sedimentary samples collected from the Marathousa 1 Area B profile (units UB10-UB1) underwent the typical procedure used for extraction of the total organic lipids (TLEs) and subsequent purification steps (e.g., Butiseacă et al., 2021) at the Senckenberg Biodiversity and Climate Research Centre (SBiK-F) in Frankfurt am Main, Germany. In short, the samples were dried, weighed, and homogenized manually using an organic solvent pre-cleaned agate mortar and pestle. Lipids were extracted using a Soxhlet apparatus with a mixture of dichloromethane and methanol (7.5:1; *v:v*) and pre-extracted cellulose thimbles. Extracts were evaporated to near dryness under continuous N_2 flow using a TurboVap LV. Subsequently elemental Sulphur was removed from the TLEs using Cu shreds activated with 10 % HCl. The vials containing TLE, activated Cu and magnetic rods were placed on a stirring table for ~20 h. Afterwards, the TLEs were filtered over a Na_2SO_4 column to remove particles, including Cu and Cu sulfides and any residual water. The solvents were evaporated using gentle N_2 flow. The desulphurization step was repeated until no reaction with the Cu was observed. Up to 50 % of the TLE was archived while the rest was further separated into fractions containing lipids of different polarity using Al_2O_3 column chromatography following the protocol detailed in Butiseacă et al. (2021).

The polar fraction containing glycerol dialkyl glycerol tetraether lipids (GDGTs) was dissolved in a 1 ml mixture of *n*-hexane (*n*-hex)/isopropanol (IPA)-(99:1; *v:v*) and dispersed using an ultrasonic bath (~30s/sample), then filtered over a 0.45 mm PTFE filter using a 1 ml syringe. The filtered polar fraction was measured using a Shimadzu HPLC, using two UHPLC silica columns (2.1 × 150 mm, 1.7 μm) in series, connected to a 2.1 × 5 mm pre-column coupled to an ABSciex 3200 QTrap chemical ionization mass spectrometer (HPLC/APCIeMS) at SBiK-F in Frankfurt am Main, Germany. The column temperature was 30 °C and flow rate was 0.2 ml/min. GDGTs were eluted isocratically using 18 % B for 25 min, then a linear gradient to 35 % B in 35 min, followed by a ramp to 100 % B in 30 min, where B is hexane/isopropanol (9:1; *v:v*) and A is hexane. For each sample a 5 μl injection volume was used and GDGT detection was achieved through single ion monitoring. Isoprenoid and branched GDGTs quantification was performed using the Sciex Analyst software and the peaks were integrated manually for each sample multiple times. An average value was calculated for the samples with multiple integrations.

The apolar fraction containing *n*-alkanes was purified using $AgNO_3$ impregnated silica column and the *n*-alkanes were later identified using the Gas Chromatography-Mass Spectrometry (GC–MS) at SBiK-F using a Thermo Scientific Trace GC Ultra - DSQII equipped with a HP-5MS column (L 30 m × D 0.25 mm × F 0.25 μm). The GC oven was held at 70 °C for 1 min, ramped at 10 °C × min^{-1} to 180 °C (5 min hold), ramped at 3 °C × min^{-1} to 320 °C (15 min hold). *n*-Alkanes were identified by comparing their retention time and mass spectrum to an external standard (Alk *n*-C_7 to *n*-C_{40}; Supelco 49,452-U, 1000 ng/μl) and quantified using peak areas calibrated against the corresponding standard *n*-alkane peak. Peak assessment and quantification were performed using the Thermo Xcalibur 2.2 SP1.48 software.

4.2.2. GDGT-based calibrations and temperatures calculation

The application of continental temperature branched (br)GDGT-based reconstruction has undergone multiple modifications since its initial use by Weijers et al. (2007) brGDGT membrane lipids were at first isolated from peat accumulations (Sinninghe Damsté et al., 2000). They have since been identified in diverse settings, including marine (Hopmans et al., 2004), soils (Weijers et al., 2007), lacustrine (Pearson et al., 2011), and riverine (De Jonge et al., 2014) locations.

The microbial producers of brGDGTs remain elusive (Sinninghe Damsté et al., 2018), therefore palaeoclimate reconstructions currently rely on empirical calibrations at both the regional and global levels as reported by Raberg et al. (2021). Given the highly changing palaeoenvironment reconstructed for Marathousa 1 (varying from lake, to delta, to flood plain, ponds and back to lake) and the impossibility to identify the exact producers in these more than 400 kyr old sediments, we used two calibrations to identify if the relative changes in the temperature record are coeval. The matter of exact palaeotemperature estimates is not fully resolved, being dependent on identifying the exact producers, unachievable for the time being in the absence of preserved palaeogenetic evidence (i.e., DNA or other distinguishing features). We will therefore focus our interpretation on the relative temperature changes and monitor their co-occurrence with other palaeoclimate proxies discussed in this contribution. Under the assumption that most of the brGDGTs from the Megalopolis Basin originated from the catchment soils, with the provision that some could have been produced within the (lake) water column, we first used the calibration of De Jonge et al. (2014). This calibration is based on a globally distributed (222) soils with the mean annual air temperature (MAAT) estimated as:

$$MAAT^{'}\,(^{\circ}C) = 7.17 + 17.8 \times [Ia] + (25.9 \times [Ib]) + (34.4 \times [Ic]) - (28.6 \times [IIa]).$$

The residual mean square error (RMSE) of this method is ±4.6 °C, where [Ia], [Ib], [Ic] and [IIa] are the fractional abundances as detailed by De Jonge et al. (2014).

Following the recent reports of lake-produced brGDGTs (e.g., Martínez-Sosa et al., 2021), we also used the calibration of Raberg et al. (2021) which is based on a revised fractional abundance related to the warm-season temperature calibration, recommended to be used in lake sediments globally, including at high latitudes (i.e., colder). The calculation of the mean annual temperature above freezing (MAF) is based on the MBT'_{5ME} index (De Jonge et al., 2014), calibrated against temperature in 182 global lake systems (Raberg et al., 2021) as:

$$MAF\,(^{\circ}C) = -0.5 + 30.4^{*}\,MBT'_{5ME}\ (\text{RMSE of } 2.32\,^{\circ}C) \text{ where.}$$

$$MBT'_{5ME} = ([Ia] + [Ib] + [Ic])/([Ia] + [Ib] + [Ic] + [IIa] + [IIb] + [IIc] + [IIIa]).$$

The decision of using the MAF calibration based of the lake-produced brGDGT (Raberg et al., 2021) was supported by the observation that the distribution of each brGDGT in Marathousa 1 was consistent with a lake origin where IIa, IIb, IIc, IIIa and IIIb are more abundant than the IIa', IIb', IIc', IIIa' and IIIb', as reported by Martínez-Sosa et al. (2021) and shown in Supplementary fig. 1, Supplementary table 3.

4.2.3. Compound specific stable isotopes

4.2.3.1. Compound specific hydrogen isotope ratios (δ^2H). The δ^2H values of *n*-alkanes were determined by GC/Thermal Conversion (TC)/ isotope ratio mass spectrometry (irMS) using a Thermo Scientific Trace 1310 GC coupled to a Thermo Scientific Delta V irMS, via an Isolink II and Conflo IVat the NIOZ Royal Netherlands Institute for Sea Research (similarly to Weiss et al., 2022). Alkane fractions were injected on a PTV injector with on-column liner – on a CP sil 5 column of 30 m length, 0.32 mm diameter and 0.4 μm film thickness using manual injection. The injection volume was approximately 1 μl, with the TC reactor set to a temperature of 1420 °C. The daily determined H_3^+ – factor was 6.1 ± 0.1 ppm mV^{-1}. Depending on the available material and reproducibility, samples were replicated up to three times, aiming for peaks of approximately 1500 to 2000 mV for compounds of interest. Hydrogen gas with a predetermined isotopic composition was used as monitoring gas and samples were only analyzed when the average difference in isotope values for *n*-alkanes from mixture B5 (Schimmelmann type A, specific for *n*-alkanes; produced by Indiana University) was less than 5 ‰ from the certified value, with a standard deviation less than 5 ‰. The δ^2H values are expressed in ‰ relative to VSMOW (Vienna Standard Mean Ocean Water) reference.

4.2.3.2. Compound specific carbon isotope ratios ($\delta^{13}C$). The carbon isotope ratios ($\delta^{13}C$) of individual *n*-alkanes were measured at NIOZ on a GC-combustion [C]-irMS using the same CP Sil 5 GC column, but with 0.12 μm film thickness and similar GC-irMS system as for ^2H analyses, now equipped with a combustion reactor. The $\delta^{13}C$ values are expressed in ‰ relative to VPDB (Vienna Peedee Belemnite) and were calculated by comparison to a CO_2 monitoring gas with a predetermined carbon isotopic composition. Every day the machine performance was checked using an in-house GC standard for chromatographic quality with 2 co-injected perdeuterated *n*-alkanes with a certified isotope composition (IAEA). Samples were analyzed at least twice (deviations ±0.3 ‰) and the same two perdeuterated *n*-alkanes were co-injected with all samples to check the machine performance.

4.2.4. Leaf waxes indices

To identify first order changes in *n*-alkanes sources and to monitor the preservation of the organic matter (targeting for a minimal alteration of the initially produced biomarkers), a number of indices were calculated as reported below.

The carbon preference index (CPI; Marzi et al., 1993) and the average chain length (ACL; Gagosian and Peltzer, 1986) were used as a primary check. To avoid an overestimation of the odd-carbon predominance and a possible asymptotic increase of one of the terms of the equation proposed by Bray and Evans (1961) if its denominator approaches zero (Herrera-Herrera et al., 2020) the relation was calculated as:

$$CPI = ((C_{23} + C_{25} + C_{27} + C_{29} + C_{31}) + (C_{25} + C_{27} + C_{29} + C_{31} + C_{33}))/(2 \times (C_{24} + C_{26} + C_{28} + C_{30} + C_{32}))$$ where C_n is the *n* – alkane with n carbon numbers.

$$ACL = ((C_{21} \times 21) + (C_{23} \times 23) + (C_{25} \times 25) + (C_{27} \times 27) + (C_{29} \times 29) + (C_{31} \times 31) + (C_{33} \times 33))/(C_{21} + C_{23} + C_{25} + C_{27} + C_{29} + C_{31} + C_{33}).$$

The aquatic plant index (P_{aq}) quantifying the different plant types (e.g., submerged vs. emerged) was calculated according to Ficken et al. (2000):

$$P_{aq} = (C_{23} + C_{25})/(C_{23} + C_{25} + C_{29} + C_{31}).$$

The grass-tree proxy was calculated using Schwark et al. (2002) as the C_{31}/C_{27} *n*-alkane ratio.

5. Results

5.1. Revised chronology

The age model of Bludau et al. (2021) placed the MAR-1 sequence between 463 ka and 427 ka. The new computed age model places the MAR-1 sequence between 485 ka and 412 ka extending the overall sequence age (Supplementary table 1), now covering not only the glacial stage of MIS 12 but the end of MIS 13 and beginning of MIS 11 interglacials as well, largely corresponding to lignite deposits, generally considered as representing warm periods (e.g., Okuda et al., 2002). The previous model by Bludau et al. (2021) did not take into account the major erosional hiatus in the middle of the sequence and instead set the starting point of the sequence much later, inside MIS12. The new model fits better with the sampled sequence that included parts of the overlying and underlying lignites. This new age model, accounting for the hiatus correction, indicates that the MIS 12b substage is missing from MAR-1 sedimentary record. The approximated ages for the respective units are shown in Fig. 2, while the input parameters in Supplementary table 2.

5.2. Temperature estimates

Regardless of the used calibration, for soils (De Jonge et al., 2014) or for lakes (Raberg et al., 2021), the reconstructed temperature varies over the studied time interval by ~5.5 °C (Fig. 3), but the important changes co-vary (i.e, the pronounced cooling and warming episodes) across calibrations. The low temperature interval overlapping with UB6 and UB5 independently confirms the sustained cold episode assigned to MIS 12. Equally, the higher temperatures associated to UB2 and UB1, support the interpretation that the lignite seam was deposited during a warm stage, in this case MIS 11.

5.2.1. Mean annual air temperature based on soil calibration

MAAT values from Marathousa 1 Area B site range between 4.5 and 10 °C (± 4.6 °C) (Fig. 3; Supplementary table 4), with an average value of 6.8 °C. The temperature decreases gradually from the base of the section (UB10, ~7.5 °C) until the middle (UB6) when it attains the minimum registered (4.5 °C), then increases again towards the top, with the maximum at sample Top125 (10 °C at ~419 ka; UB2). The cooling interval is punctuated by two small warmings, one in UB8 (BC_145 sample, ~471 ka; 8.4 °C) and another one peaking at the UB7 – UB6 transition (BC_0 sample, ~436.8 ka; 8.0 °C). The interval between UB6 and the base of UB4 is marked by a sustained cooling episode with an average MAAT value of 5.2 °C, corresponding to the glacial maximum (at ~436–432 ka). After this interval, MAAT follows an overall warming trend towards the top, to reach the overall maximum in the section (in the top of UB2). Temperatures remain high (with an average value of 9.1 °C) over the entire UB1 unit, when another cooling period seems to start at the very top of the section (Top25 sample, ~413 ka; 6.7 °C). The archaeological horizon is characterized by MAATs between 5 and 6.8 °C, with an average value of 5.7 °C.

5.2.2. Mean annual temperature above freezing based on lake calibration

MAF values vary between 9.4 °C and 15 °C, with an average of 11.7 °C (Fig. 3; Supplementary table 4). Overall, MAF follows a similar trend as MAAT through the section, except for samples 351_30 –

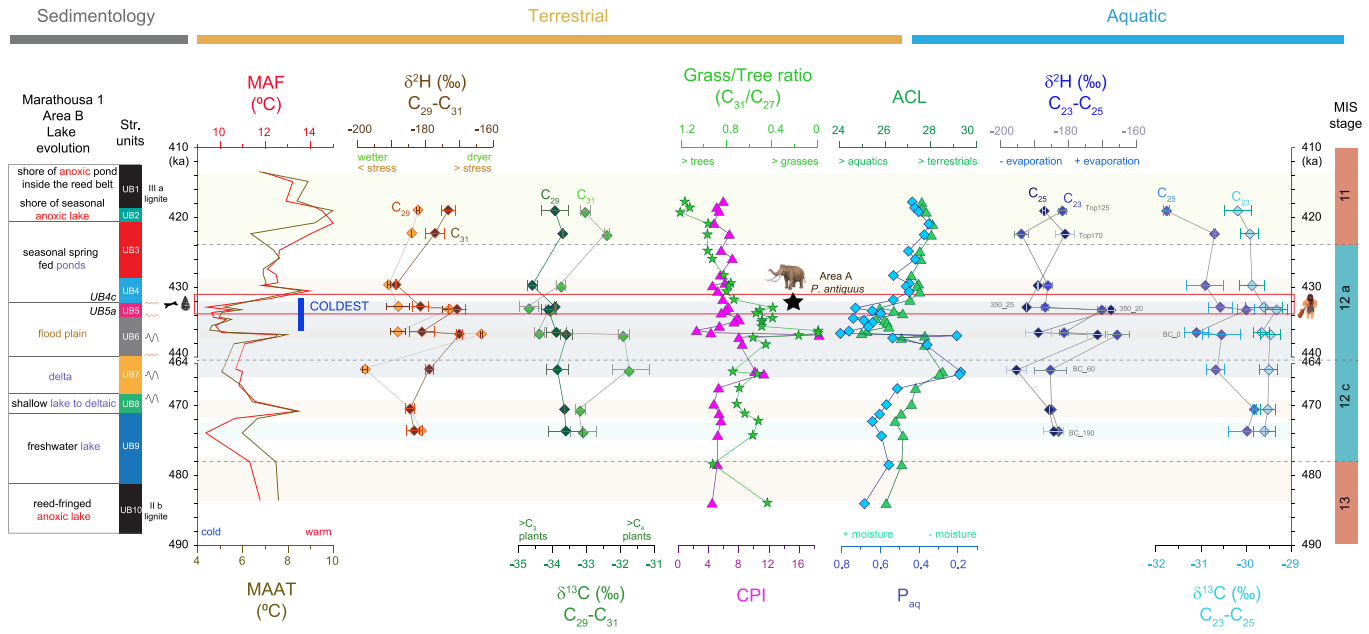

Fig. 3. Biomarker and stable isotope results from Marathousa 1 site. From left to right: Area B Lake evolution and sedimentological units (Bludau et al., 2021); MAF = mean temperature above freezing; MAAT = annual air temperature; $\delta^2H_{C29\text{-}C31}$ = hydrogen isotopic composition of C_{29} and C_{31} *n*-alkanes; $\delta^{13}C_{C29\text{-}C31}$ = carbon isotopic composition of C_{29} and C_{31} *n*-alkanes; Grass/Trees ratio (C_{31}/C_{27}); CPI = Carbon Preference Index; ACL = Average Chain Length of *n*-alkanes; P_{aq} = Aquatic Plants Index; $\delta^2H_{C23\text{-}C25}$ = hydrogen isotopic composition of C_{23} and C_{25} *n*-alkanes; $\delta^{13}C_{C23\text{-}C25}$ = carbon isotopic composition of C_{23} and C_{25} *n*-alkanes. On the right side of the figure are marked the MIS divisions and subdivisions (Lisiecki and Raymo, 2005). Pale blue and orange horizontal panels represent periods of warming and cooling. With red rectangle and associated symbols is marked the archaeological interval. Additionally, on the top of the figure are represented with colored bars the sedimentological markers (grey) and terrestrial (orange) and aquatic signals (blue bar). The black star represents the area A correspondent of the archaeological level with isotope measurements on *P. antiquus* tooth (Roditi et al., 2024). (For interpretation of the references to colour in this figure legend, the reader is referred to the web version of this article.)

Top170 (424–422 ka), when MAAT values increase slightly earlier. MAF values are ~5 °C higher than MAAT values, with the lowest temperatures registered in the interval between ~436–432 ka. The archaeological horizon is characterized by MAFs between 9.4 and 12.1 °C, with an average value of 10.4 °C. The minimum value in the section corresponds to sample 350_25, at ~432.8 ka, towards the end of the glacial maximum.

5.3. Isotope measurements

5.3.1. Leaf wax hydrogen isotopic compositions ($\delta^2H_{n\text{-}alkanes}$)

n-Alkanes ranging from *n*-C_{17} to *n*-C_{35} with a strong odd-over-even predominance were identified throughout the sample set, and stable hydrogen isotope values (δ^2H) are reported only for the higher amplitude C_{23} to C_{31} peaks. δ^2H values of C_{23} *n*-alkanes ($\delta^2H_{C23n\text{-}alkanes}$) range from −165.5 ‰ to −194 ‰ (Fig. 3; Supplementary table 5) with an average value of −181.8 ‰. $\delta^2H_{C23n\text{-}alkanes}$ values show two strong positive shifts, one of ~20 ‰ at 436.8 ka (from −185 ‰ –165.5 ‰; the highest in the section; sample BC 0; UB6) and a second one of at 433.2 ka 11 ‰ (from −181 ‰ to −170 ‰; sample 350_20; UB5), at the beginning of the archaeological horizon. A negative shift of ~8 ‰ is also registered at 422.3 ka (from −186 ‰ to −194 ‰; the minimum registered in the area; sample Top170; UB3), followed by an increase in values close to the average. $\delta^2H_{C25n\text{-}alkanes}$ values vary between −167 ‰ and − 195 ‰ (Fig. 3; Supplementary table 5) with an average value of −184 ‰. $\delta^2H_{C25n\text{-}alkanes}$ values co-vary with their $\delta^2H_{C23n\text{-}alkanes}$ homologues until ~422 ka (UB3), when they start to show opposing trends.

$\delta^2H_{C29n\text{-}alkanes}$ values fall between −197.7 ‰ to −163.4 ‰, with a mean value of −183.3 ‰. Isotopic values are decreasing from −181 ‰ at ~473 ka (UB9) to −197.7 ‰ at ~465 ka (UB7, sample BC_60; the lowest value measured; Supplementary table 5), followed by two positive shifts at 436.8 ka to −163.4 ‰ (BC_0 sample; UB6) and at ~433.2 ka to −172.9 ‰ (sample 350_20; UB5). $\delta^2H_{C29n\text{-}alkanes}$ values decrease again until 429.7 ka (−190.8 ‰), then slightly increase towards the end of the section. $\delta^2H_{C31n\text{-}alkanes}$ co-vary with $\delta^2H_{C29n\text{-}alkanes}$, but with values consistently slightly less negative (Fig. 3; Supplementary table 5).

5.3.2. Leaf wax carbon isotopic compositions ($\delta^{13}C_{n\text{-}alkanes}$)

The $\delta^{13}C$ values of C_{23} *n*-alkanes ($\delta^{13}C_{C23n\text{-}alkanes}$) vary between −30.2 ‰ and − 29.3 ‰ (Fig. 3; Supplementary table 6), with a mean value of −29.7 ‰. $\delta^{13}C_{C23n\text{-}alkanes}$ values are constant from the bottom of the section until 436.8 ka when a small negative excursion of 0.3 ‰ occurs (sample BC_0; UB6), followed by an immediate increase of 0.3 ‰ before the archaeological horizon (sample 349_70, same unit; 436.5 ka). From the archaeological horizon until the top of the section $\delta^{13}C_{C23n\text{-}alkanes}$ values are decreasing gradually, from −29.3 ‰ (sample 350_20, 433.2 ka; UB5) to −30.2 ‰ (the lowest registered value; sample Top125, 419 ka; UB2). The $\delta^{13}C_{C25n\text{-}alkanes}$ vary between −31.8 ‰ and − 29.8 ‰ (Fig. 3; Supplementary table 6), with an average of −30.6 ‰. $\delta^{13}C_{C25n\text{-}alkanes}$ values co-vary in general with $\delta^{13}C_{C23n\text{-}alkanes}$, but with a more pronounced negative trend. Within the archaeological horizon there is a positive shift of 1.1 ‰ in the $\delta^{13}C_{C25n\text{-}alkanes}$ values, from −31.1 ‰ to −30.0 ‰ (between 436.5 and 433.2 ka).

For $\delta^{13}C_{C29n\text{-}alkanes}$ the values vary from −34.7 ‰ to −31.7 ‰ (Fig. 3; Supplementary table 6), with a mean value of −33.2 ‰. A major shift of −2.5 ‰ is recorded at ~436 ka (between BC_0 and 349_70 samples; UB6), followed by a short positive excursion of 0.2 ‰ at 433.2 ka (sample 350_20; UB5). At the level of the archaeological horizon (sample 350_25, 432.8 ka; UB5), the $\delta^{13}C_{C29n\text{-}alkanes}$ attains the minimum value in the section, after which a progressive increase of 2.3 ‰ characterizes the top-half of the section. $\delta^{13}C_{C31n\text{-}alkanes}$ are decoupled from the $\delta^{13}C_{C29n\text{-}alkanes}$ values, except for the base and the top of the section, where they co-vary. $\delta^{13}C_{C31n\text{-}alkanes}$ values are less variable and remain around an average value of −33.9 ‰.

5.4. n-Alkane indices

The CPI values range between 2.4 and 18.6, with an average value of 6.5 (Fig. 3, Supplementary table 4). A high variability interval is documented between ~466 and 432 ka. The minimum attained value occurs in UB6 at ~435 ka (samples 349_70 – 349_75), while the highest value is registered at the middle of UB6 at 436.8 ka (sample BC 0). For the archaeological horizon values range between 5.68 and 6.63, with an average value of 6.10.

ACL index shows values between ~24.9 and 28.4, with a mean value of 26.9 (Fig. 3, Supplementary table 4). The general trend indicates a slight increase from the base of the section towards the top, except for the interval between ~464 and 432 ka (UB7 – UB5). This interval is characterized by large amplitude values just as the CPI, with short periods of indicative increased aquatic components (values of ~25). ACL values within the archaeological horizon vary between ~25.7 and 26.7.

P_{aq} ranges between 0.19 and 0.81, with an average value of 0.52 (Fig. 3, Supplementary table 4). Values show an overall decreasing trend from the base of the section until ~465 ka (samples BC_55, BC_60). In the interval between 465 and 436 ka P_{aq} values register a high variability, including the minimum and maximum attained in the section. Above this level, it follows an overall decreasing trend towards the top of the section. Between ~436–433 calculated P_{aq} values are the highest in the section. Within the archaeological interval values vary between 0.53 and 0.73, with an average value of 0.62.

The grass vs. tree ratio (C_{31}/C_{27}) varies between 0.8 and 5.8, with a mean value of 1.68. In the interval between ~440–432 ka (units UB6 – UB5) there is an increase in values that corresponds to the glacial maximum and the archaeological horizon. The highest value is registered in BC_0 sample, at 436.8 ka.

6. Discussion

MIS 12 represents one of the most severe Quaternary 'long glacial' periods (Lisiecki and Raymo, 2005), with large active ice caps and mountain glaciers, including in the mountains of Greece and Peloponnese(Hughes et al., 2006; Leontaritis et al., 2020). Such prolonged cold climatic conditions must have impacted biota in general, as well as hominin survival in the area.

6.1. Temperature variation

Marathousa 1 Area B continental temperatures estimates follow an overall decreasing trend from the base of the section until ~432 ka (Fig. 3). A sustained cold period is observed in the section between ~436–432 ka, identified as the glacial maximum or the peak of the MIS12 glacial period. Early humans are present at the MAR-1 location in a window of ~3 kyr, at the end of the glacial maximum (~434–432 ka; UB5 – UB4 contact), suggesting the potential shelter role of Megalopolis Basin during the harsh conditions associated with the glacial peak.

An important part of the section was deposited during glacial conditions, with brGDGT production (i.e., MAAT calculation) being influenced by the changing conditions, with soils forming at a lower rate during the times of prolonged low temperatures. However, most of the existing continental palaeotemperature records until recently (Martínez-Sosa et al., 2021; Raberg et al., 2021) used MAAT estimates based on the calibrations developed by De Jonge et al. (2014). Since the increased recognition that lake produced brGDGTs are frequently contributors to the entire GDGT pool and the known effect of freezing season altering the produced temperature estimates (Martínez-Sosa et al., 2021; Raberg et al., 2021; Ramos-Román et al., 2022), the brGDGT based MAF was further used in this study. The calculated continental temperatures follow the same trend, but MAF values are overall 5 °C higher than MAAT. The largest difference between the two calibrations is at ~422 ka (+7 °C instead of the regular +5 °C) at the MIS12 – MIS11 transition), appearing at a regime change, from the cold glacial to the warmer interglacial. In this specific case, we suspect that the production and preservation of the brGDGTs do not linearly respond to the changes in continental temperature but are influenced by locally changing environmental conditions.

6.2. Vegetation response to water availability and temperature changes

Plant waxes (among them *n*-alkanes) are found in the cuticles of vascular plants (Eglinton and Hamilton, 1967), their main role being the prevention and regulation of water loss. For terrestrial plants, the enrichment in deuterium (^2H) occurs from direct transpiration at the leaf level, evaporation of soil water (Flanagan et al., 1991), or intake from precipitation or atmospheric vapor (Sachse et al., 2012). In the case of aquatic plants, the source of δ^2H is the water in the aquatic environment they live in. The discrimination against ^2H during photosynthesis is greater in C_3 plants than in C_4 plants (e.g., Eglinton and Eglinton, 2008; Feakins and Sessions, 2010). In arid environments (both hot or cold) the δ^2H changes towards more ^2H enrichments as a function of evaporation. Due to their capacity of retaining the water signal, as well as their wide distribution and general good preservation in sedimentological records, leaf waxes are important tools for palaeoclimate and palaeohydrology reconstructions (Liu et al., 2006; Sachse et al., 2012; Gaviria-Lugo et al., 2023). Higher $\delta^2H_{n\text{-alkanes}}$ values correspond to low water intake/increased evaporation, while lower $\delta^2H_{n\text{-alkanes}}$ to higher water intake/increased precipitation, respectively.

Marathousa 1 $\delta^2H_{C29\text{-}C31 n\text{-alkanes}}$ data indicate two drier episodes, the first one associated with a short-term warming peak at ~436.8 ka (BC_0 sample; UB6) with $\delta^2H_{C29 n\text{-alkanes}}$ values of −163 ‰ and $\delta^2H_{C31 n\text{-alkanes}}$ of −170 ‰, while the second one, at ~433.2 ka (sample 350_20; UB5), attains $\delta^2H_{C29\ n\text{-alkanes}}$ values of −172.8 ‰ and $\delta^2H_{C31 n\text{-alkanes}}$ of −170.6 ‰ (Figs. 3, 4). This second important dry peak is associated with the end of the MIS 12 glacial maximum, and it corresponds to the lower part of the archaeological horizon (UB5a; Fig. 3). The high values can be linked to increased evaporation or/and low precipitation values, pointing to a moisture deficiency affecting the basin catchment during those particular timespans. For the same intervals, similar values are registered by $\delta^2H_{C23\text{-}25 n\text{-alkanes}}$ (*n*-alkanes specific to water-loving plants, i.e., reeds, mosses, submerged and floating plants; $\delta^2H_{C23 n\text{-alkanes}}$ of −170 ‰; $\delta^2H_{C25 n\text{-alkanes}}$ of −167.3 ‰), indicating that aquatic plants growing in and around the lake were using water with increased δ^2H, linked to prevailing evaporation, or meltwater inputs from higher elevations (as suggested by Bludau et al., 2021). P_{aq} shows an overall decreasing trend until ~436 ka, indicative of a more negative water balance. Between ~436–432 ka (UB6 – UB5; Fig. 3), the proxy values are increasing considerably, suggesting an increase in moisture and/or water availability at the section location. The Mg/Ti ratio also drops during the glacial, indicating a reduction in alkalinity corroborated with an increase in erosion (i.e., increase in Rb/Sr ratio; Bludau et al., 2021).

The increasing values of $\delta^{13}C_{C31 n\text{-alkanes}}$ (C_{31} more abundant in grasses) to the detriment of $\delta^{13}C_{C29 n\text{-alkanes}}$ (C_{29} more abundant in trees) from ~465 to 436 ka points towards an increase in C_4 plant contribution indicating an opening of the landscape, with elevated presence of grassy elements (Fig. 3; Supplementary table 6). The grass/tree ratio values (Fig. 3; Supplementary table 4) show that C_4 vegetation contribution remains important in Megalopolis until the archaeological level (~432 ka; Fig. 3). $\delta^{13}C_{enamel}$ values of the *Palaeoloxodon antiquus* in area A (Roditi et al., 2024) also show that the animal fed on a mesic/open woodland vegetation. Based on the sedimentological and micropalaeontological records, Bludau et al. (2021) suggest a transition from an open lake environment to a proximal deltaic system and then to a flood plain. An open flat landscape would have provided easy access to available resources for the hominin population(s) in the area, as well as for the rest of the animals.

For the remainder of the section, the trend in isotopic values is similar, except for the $\delta^2H_{C23 n\text{-alkanes}}$, which values behave completely opposite to the rest of the proxies after ~422.3 ka (after UB3 – UB2

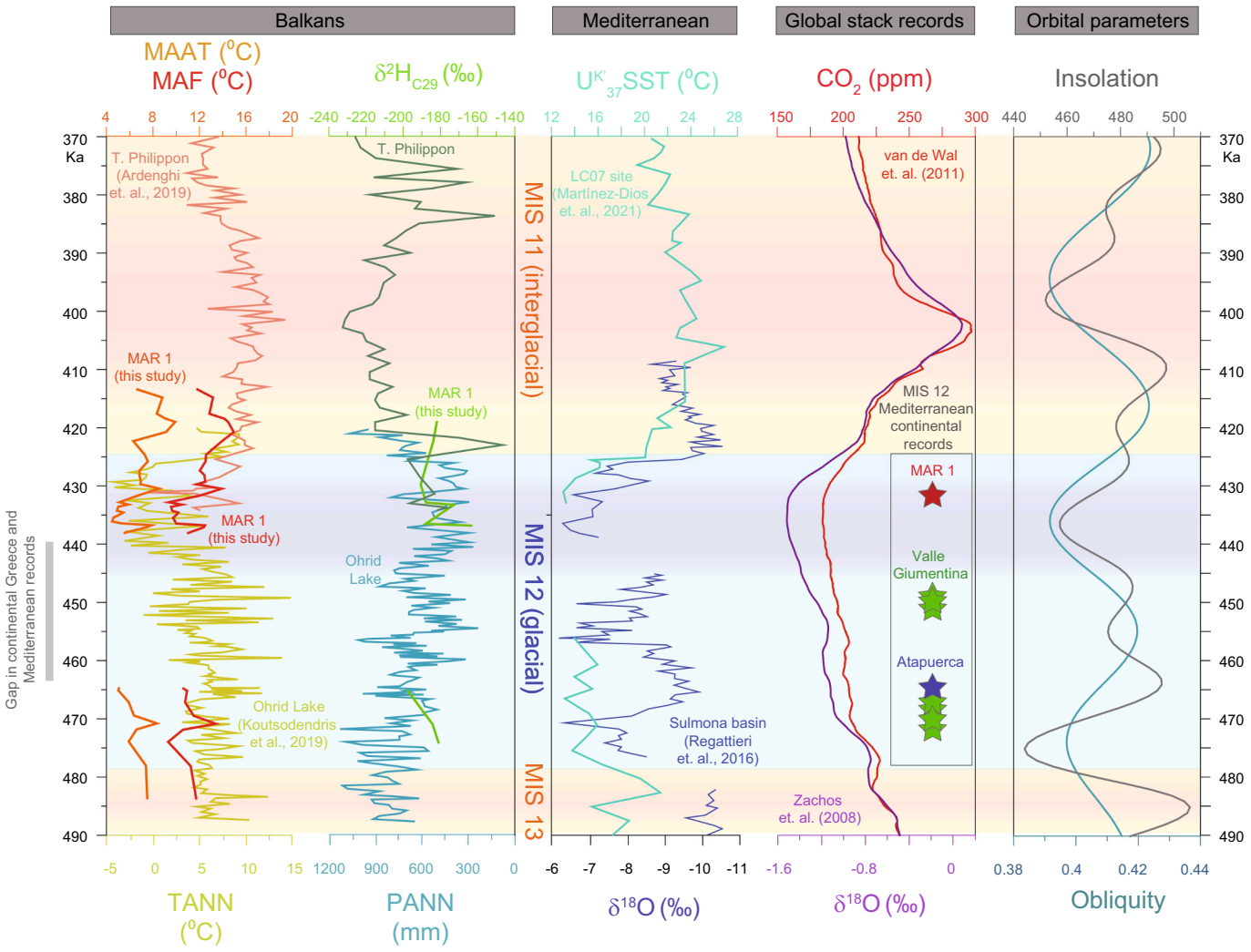

Fig. 4. Composite records for MIS 11 and MIS 12 for Balkans, Mediterranean, Global stacks and Orbital parameters. From left to right: MAAT = mean annual air temperature (Tenaghi Phillipon site, Northern Greece; Ardenghi et al., 2019 and MAR 1- this study); MAF (this study); TANN = pollen based mean annual temperature (Ohrid, Koutsodendris et al., 2019); δ^2H_{C29} = hydrogen isotopic composition of C_{29} *n*-alkanes (Tenaghi Phillipon site, N. Greece; Ardenghi et al., 2019; MAR 1- this study); PANN = pollen based mean annual precipitations (Ohrid, Koutsodendris et al., 2019); $U^{K'}_{37}$SST = alkenones based sea surface temperature (MD81-LC07 core, Sicily Straight; Martínez-Dios et al., 2021); $\delta^{18}O$ = oxygen isotopic on lake carbonates in Sulmona Basin (Regattieri et al., 2016); CO_2 = carbon dioxide concentration (global stack; van de Wal et al., 2011); $\delta^{18}O$ = oxygen isotopic composition (global stack; Zachos et al., 2008); Insolation and Obliquity curves. With colored stars on the right side are marked MIS 12 continental archaeological sites in the Mediterranean area.

contact; Fig. 3) indicating changing conditions possibly associated to the transition into the (wetter) MIS 11 interglacial (at ~424 ka) and to the presence of seasonally isolated ponds as reconstructed by Bludau et al. (2021). Most probably, the section was located in one of these ponds/small lakes between ~425–418 ka. C_{23} is dominant in moss and reeds, prevailing in *Sphagnum* moss, which prefers colder and humid conditions. Major changes in $\delta^2H_{C23n\text{-alkanes}}$ points to major changes in water availability.

Micropalaeontological data suggest a generally shallow environment at the MAR-1 location, with a low abundance of microfauna (Bludau et al., 2021). However, the number of sponge (the most abundant micro taxa) spicules increases in the upper part of the section, probably as a response to increasing temperatures (as confirmed by the reconstructed MAATs and MAFs) and nutrients. Ostracods are also more abundant in the upper part, but only between ~432–425 ka. Temperatures calculated based on ostracods range between 10.5 °C and 18 °C (Bludau et al., 2021), close to the calculated 9.4 to 15 °C MAF values. All sponges and ostracods species described in MAR-1 are freshwater taxa, characteristic to lakes and riverine systems (Bludau et al., 2021).

6.3. *n*-Alkanes sources and distribution

The Marathousa 1 samples contain *n*-alkanes with chain lengths between C_{16}–C_{35}, with a predominance of C_{21}–C_{33} (Supplementary fig. 2), with *n*-alkanes shorter than C_{15} or longer C_{36}–C_{40} below the detection limit. *n*-Alkane homologues with chain lengths shorter than *n*-C_{21} are produced principally by aquatic elements such as algae and submerged plants. Higher homologues (e.g., *n*-C_{21} and *n*-C_{23}) are preferentially produced by macrophytes, reeds and mosses, while above *n*-C_{27} predominantly by herbaceous plants and trees (Ficken et al., 2000). The most abundant *n*-alkanes (i.e., C_{21}–C_{33}) indicate that main sources of *n*-alkanes in the record were terrestrial and semi-aquatic plants, and subsequently submerged plants and algae (Supplementary fig. 2).

n-Alkanes are highly abundant and well-preserved throughout the record, except for a few samples (BC 60; BC 55 BC 15; BC 0; 349_95 and 350_25), correlated with the glacial maximum (~465–432 ka; top UB7 – UB5), with low temperatures and general drier conditions (Fig. 3). At 436.8 ka (sample BC 0; UB 6), where a short and abrupt warm event is registered and marked in the lithological record by an erosional surface (Karkanas et al., 2018), is particularly dominated by long chain *n*-

alkanes, pushing both the CPI and ACL to higher values, consistent with drier conditions as suggested by the $\delta^2H_{C29\text{-}C31 n\text{-alkanes}}$.

Between 436.5 and 435.5 ka, the samples immediately after BC 0 (349_70 – 349_85) exhibit the lowest CPI values in the section (~2.4–5.4). Low CPI values can be associated with microbial degradation under very low sedimentation rates (Duncan et al., 2019), or organic matter degradation in general (Angst et al., 2016). Low CPI ratios also translate into low biogenic input and increased petrogenic contribution (Pendoley, 1992), indicating low *n*-alkane production and reworking for this time interval. Grain size analysis revealed a dominance in coarse material for UB7 and UB6 units (Bludau et al., 2021), associated with an overall increase in dust and terrestrial material input (i.e., increased Ti and La concentrations; Bludau et al., 2021. Karkanas et al. (2018) discuss the possible link between increased carbonate content and clast input due to enhanced mechanical erosion, which could be related to increased aridity/reduced forest cover. The TOC (total organic carbon) and C/N (carbon to nitrogen ratio) measured by Bludau et al. (2021) also decrease with the glacial maximum onset, interpreted as a low energy indicator. The association of lower ACL values with high P_{aq} values during the coldest MIS 12 interval indicate a significant input from submerged/floating plants (Ficken et al., 2000), suggesting lake shrinkage and less precipitation for the same time interval. Collectively, the environmental proxies show cold and dry conditions at the archaeological horizon deposition in the beginning (UB5a), that change to milder towards the upper part (UB4c).

6.4. Temperature and humidity variations in regional and global context

Marathousa 1 provides the most complete, high-resolution continental temperature record for MIS 12 in Greece and the Mediterranean area, particularly important in the context of human populations presence. Prolonged, low temperatures (i.e., glacial maximum) at Marathousa 1 were recorded between ~436–432 ka (UB6 – UB5, overlapping with most of the archaeological horizon; MIS 12a), in accordance with the global minimum records (e.g., Lisiecki and Raymo, 2005; Koutsodendris et al., 2019). Pollen data collected around the Megalopolis basin (Okuda et al., 2002), from Tenaghi Philippon (Tzedakis et al., 2006), and from Lake Ohrid (Koutsodendris et al., 2019) show a decrease in mesophilous taxa during this time interval and an increase in steppe elements, information supported by our increasing $\delta^{13}C_{n\text{-alkanes}}$ values, pointing to an increase in C_4 plants and/or water stress.

When comparing our temperature records with reconstructed pollen-based temperature estimates from Lake Ohrid (Balkans, Fig. 1; Koutsodendris et al., 2019) for the same time interval, MAAT shows temperatures of ~5 °C lower temperature in Marathousa 1, with the exception of the coldest phase of MIS 12 (Fig. 4), when Ohrid shows close to 0 °C (Fig. 4). The Tenaghi Philippon biomarker record (Greece, Ardenghi et al., 2019) partially overlaps with Marathousa 1 between 415 and 434 ka and shows a similar warming trends towards MIS 11, but the calculated values for Tenaghi Philippon are ~5 °C lower than soil-based calibration MAAT. Ardenghi et al. (2019) report temperature values from Tenaghi Philippon which they obtained by using the calibration proposed by Sun et al. (2011) with a better correlation to warmer season. These values are comparable to our MAF estimates (Fig. 4), which use the more recently developed lake-based calibration for months above freezing (Raberg et al., 2021). We acknowledge that utilizing estimates from different calibrations makes intercomparison of data challenging, especially when referring to absolute values. Moreover, the calibration of Raberg et al. (2021) used for Marathousa 1 is based on the improved analytical methods that have allowed for a better separation of the structural isomers (Martínez-Sosa et al., 2021). The differences in reconstructed temperatures are the result of the cumulative effect of methodological differences (i.e., molecular proxies versus pollen) and the applied biomarker-based calibrations temperature estimates. The key difference, however, arises from variations in altitude and geographical position of the different sampled sites. Lake Ohrid (the deepest lake in Europe; − 288 m) is the northernmost of all the available continental records considered here, at an elevation of ~700 m, surrounded by the central Balkan Mountains. Tenaghi Philippon is a small open peat area, ~ 40 m elevation and situated close to sea. In contrast, the Megalopolis basin is an intermontane basin, with an average elevation of ~350 m and situated almost four degrees latitude south of Tenaghi Philippon.

Regardless of the differences in palaeogeography for the mentioned sites and of the diverse methodology and calibration used for the brGDGTs temperature reconstruction, the compared reconstructed temperature records follow the same trend, with the lowest values between ~440–430 ka (Fig. 4), corresponding to the end of MIS 12 glacial and warming during the MIS 11 interglacial. All brGDGTs based temperature reconstructions are consistent in estimating an ~5 °C increase in temperature from the glacial MIS 12 to the MIS 11 interglacial.

Similar trends are also registered in precipitation (i.e., pollen-based values from Lake Ohrid; Koutsodendris et al., 2019) and hydrogen isotopic composition of *n*-alkanes (this study; Tenaghi Philippon of Ardenghi et al., 2019). Mean annual pollen-based precipitation (PANN) and $\delta^2H_{C29n\text{-alkanes}}$ values show an important drop in humidity during the MIS 12 glacial maximum (Fig. 4) and immediately after the MIS 11 onset, when temperatures are increasing abruptly. The same situation is registered also in Italy, in the Sulmona Basin, where $\delta^{18}O$ values from lake carbonates indicate a pronounced decrease of regional precipitation consistent with the MIS 12 glacial maximum (Regattieri et al., 2016; Fig. 4). Overall, at Marathousa 1 we identify an early glacial humidification (up to ~460 ka), a mid-glacial aridification (~440–432 ka), late glacial humidification (~ 432–428 ka), and again aridification into MIS 11 (after 424 ka) indicating a bi-phase hydroclimatic pattern, pointing to orbital forcing (i.e., obliquity and insolation; Fig. 4).

Even though the Marathousa 1 temperatures are low during MIS 12 (avg. MAAT of ~7 °C and MAF of 11.7 °C), the conditions in the basin are overall milder than in the surrounding areas which were covered by glaciers at high elevations (Leontaritis et al., 2020). Notably, the most extensive glaciation identified in Greece is attributed to MIS 12 and it is associated with the coldest mean summer temperatures recorded in Greece during at least the last 430 ka (≤ 4.9 °C at an altitude of 1741 m above sea level; Hughes et al., 2007). At Ioannina, situated at an altitude comparable to that of Megalopolis (ca. 480 m above sea level), the climate during MIS 12 would have been marked by mean summer temperatures of ≤12.4 °C (close to the ~10 °C from MAF of Marathousa; Fig. 3) and mean winter temperatures likely lower than −0.8 °C (Hughes et al., 2007). U^K_{37} based sea surface temperatures (SSTs) from the Sicily straight (488 m water depth; 12.20–13.30 m core depth; Martínez-Dios et al., 2021) provide values between 13 °C and 20 °C for MIS 12 in the central Mediterranean, similar to the more northern Marathousa 1 MAF record (Figs. 3; 4).

All analyzed Mediterranean records (e.g., Greece and central Mediterranean) display sedimentary hiatuses between ~465–440 ka. This indicates that climatic changes during MIS 12 glacial period had a regional influence on the sedimentary processes, possibly corresponding to increased aerial exposure (i.e., erosion under colder and drier conditions; Regattieri et al., 2016) and general sediment starvation due to low precipitation input (i.e., less riverine input). Other authors (e.g., Vidal et al., 1997; Poli et al., 2000) proposed that thermohaline circulation in the northern Atlantic stopped completely during the MIS 12 glacial maximum due to large ice volume accumulation which suppressed deep water convection (Poli et al., 2000). In the Mediterranean area, which is under the influence of NAO, this would translate into reduced vapor transport and further reduced rainfall.

Nevertheless, the large scale of the glaciation impacted the entire northern hemisphere, inducing important changes in temperature, ice-sheets expansion, sea level and associated atmospheric pCO_2. During MIS 12, temperatures and atmospheric pCO_2 dropped substantially (e.g., Zachos et al., 2008; van de Wal et al., 2011; Fig. 4), affecting both

marine and continental biota. Additionally, at ~430 ka, the onset of Mid-Brunhes Event takes place, a climatic shift between ~430 and 425 ka (MIS 12 to MIS 11 transition), which corresponds to an increase in amplitude of glacial-interglacial cycles (e.g., Raymo et al., 2007; Clark et al., 2006). After 430 ka (MIS 11), interglacials were characterized by higher temperatures and higher concentrations of atmospheric CO_2 (Jouzel et al., 2007; Lüthi et al., 2008). Mediterranean and Balkan records follow the global perspective, with MIS 12 being characterized by general low temperature and reduced humidity as the water was trapped in the regional glaciers and polar icecaps, while MIS 11 is characterized by high temperatures and increased humidity (Fig. 4 and cited references).

6.5. Hominin populations in the Mediterranean during the MIS 12 glacial

The documented hominin presence in Marathousa 1 correlates with the end of the MIS 12 glacial maximum, the MIS 12a substage. Our general environmental data show a cold and dry environment at the archaeological horizon (top UB5a), that changes to milder towards the upper part (UB4c). Other continental archaeological sites from MIS 12 (Fig. 4) are documented only in the western Mediterranean, in central Italy (Valle Giumentina; Villa et al., 2016) and northern Spain (Atapuerca; Falguères et al., 2013). The Valle Giumentina record has multiple levels of habitation between ~470–450 ka (MIS 12b, c), while Atapuerca is dated around 465 ka (MIS 12c).

Preliminary ages from other recently identified archaeological sites in the Megalopolis lignite mine (Karkanas et al., 2024) indicate the presence of hominins in the basin during other MIS stages as well between circa 700–300 ka (roughly MIS 16 to MIS 8). The evidence of human activities in glacial intervals though (i.e., Marathousa 1 site), suggests their persistence in the area through highly fluctuating climatic and environmental conditions. This could be explained by the sheltered nature of the basin (i.e., an intramontane basin), attenuating the severity of glacial conditions observed in other regions (e.g., Bludau et al., 2021).

7. Conclusions

The integrated biomarker and stable isotope leaf wax records from Marathousa 1 (Peloponnese, Greece) cover the interval between ~485–412 ka, confirming glacial conditions in southern Greece and the Eastern Mediterranean during MIS 12 stage. Biomarker-based reconstructed mean annual temperatures show a general cooling trend in the section, that culminates between ~440–432 ka, when the minimum is registered (i.e., during peak glacial conditions). This cooling is associated with important changes in vegetation, from more forested to more open landscapes (increase in C_4 plants), as well as in water and moisture availability (i.e., dryer, lake shrinkage). δ^2H values of leaf waxes indicate two episodes with drier conditions in the Megalopolis basin, one peaking at ~436.8 ka and the other at ~433.2 ka. The first is associated with a warming interval during the general cold conditions, while the second coincides with the end of the glacial maximum. The onset of sustained glacial conditions in the basin at ~465 ka (UB7) is marked by a negative excursion in the leaf wax hydrogen isotope ratio suggesting increased humidity (i.e., increased precipitations). By the end of this interval (~432 ka), the humidity drops considerably, drought affecting both terrestrial and aquatic ecosystems due to the large moisture quantity stored now in ice.

Our data also show a regional response of biota (i.e., vegetation, hydrology, animals/humans) to a global event (i.e., MIS 12 northern hemisphere glaciation), bringing new insights into the expression of this event in southern Greece and eastern Mediterranean, with major consequences over both continental and marine domains. The final part of the glacial maximum (434–431 ka; UB5a – UB4c), an interval marked by the most drastic environmental conditions observed in Marathousa 1 section, is associated with the level of human occupation, indicating that Pleistocene hominins were present in the basin at this time and supporting the role of the basin as a glacial refugium.

Credit authorship contribution statement

Geanina A. Butiseacă: Writing – review & editing, Writing – original draft, Visualization, Methodology, Investigation, Formal analysis, Data curation, Conceptualization. **Iuliana Vasiliev:** Writing – review & editing, Visualization, Validation, Supervision, Methodology, Conceptualization. **Marcel T.J. van der Meer:** Writing – review & editing, Validation, Methodology. **Ines J.E. Bludau:** Writing – review & editing, Visualization, Methodology. **Panagiotis Karkanas:** Writing – review & editing, Visualization, Validation, Methodology. **Vangelis Tourloukis:** Writing – review & editing, Funding acquisition. **Annett Junginger:** Writing – review & editing, Visualization, Investigation. **Andreas Mulch:** Writing – review & editing, Resources. **Eleni Panagopoulou:** Resources. **Katerina Harvati:** Writing – review & editing, Supervision, Project administration, Funding acquisition.

Declaration of competing interest

The authors declare that they have no known competing financial interests or personal relationships that could have appeared to influence the work reported in this paper.

Data availability

Data will be made available on request.

Acknowledgements

This research was supported by DFG (2021 Gottfried Wilhelm Leibniz Prize awarded to K. Harvati). The excavation of Marathousa 1 was conducted under the auspices of the Ephorate of Palaeoanthropology and Speleology, Greek Ministry of Culture and Sports and was financed by the European Research Council (ERC-StG-283503 'PaGE' and ERC-CoG-724703 'CROSSROADS', awarded to K. Harvati). KH is additionally supported by the ERC-AdG-101019659. KH and VT are also supported by the DFG (HA 5258/20-1|TO 1474/1-1). We thank U. Treffert for organic geochemistry laboratory support in Frankfurt.

Appendix A. Supplementary data

Supplementary data to this article can be found online at https://doi.org/10.1016/j.gloplacha.2024.104585.

References

Angst, G., John, S., Müeller, C.W., Kogel-Knabner, I., Rethemeyer, J., 2016. Tracing the sources and spatial distribution of organic carbon in subsoils using a multi biomarker approach. Sci. Rep. 6, 29478.

Ardenghi, N., Mulch, A., Koutsodendris, A., Pross, J., Kahmen, A., Niedermeyer, E.M., 2019. Temperature and moisture variability in the eastern Mediterranean region during Marine Isotope Stages 11–10 based on biomarker analysis of the Tenaghi Philippon peat deposit. Quat. Sci. Rev. 225, 105977. http://www.sciencedirect.com/science/article/pii/S0277379119304573.

Blackwell, B.A.B., Sakhrani, N., Singh, I.K., Gopalkrishna, K.K., Tourloukis, V., Panagopoulou, E., et al., 2018. ESR Dating Ungulate Teeth and Molluscs from the Paleolithic Site Marathousa 1, Megalopolis Basin, Greece. Quaternary 1, 22. https://doi.org/10.3390/quat1030022.

Bludau, I.J.E., Papadopoulou, P., Iliopoulos, G., Weiss, M., Schnabel, E., Thompson, N., Tourloukis, V., Zachow, C., Kyrikou, S., Konidaris, G.E., Karkanas, P., Panagopoulou, E., Harvati, K., Junginger, A., 2021. Lake-Level changes and their Paleo-Climatic Implications at the MIS12 lower Paleolithic (Middle Pleistocene) Site Marathousa 1, Greece. Front. Earth Sci. 9, 668445 https://doi.org/10.3389/feart.2021.668445.

Bray, E.E., Evans, E.D., 1961. Distribution of n-paraffins as a clue to recognition of source beds. Geochim. Cosmochim. Acta 22, 2–15.

Butiseacă, G.A., Vasiliev, I., van der Meer, M.T.J., Krijgsman, W., Palcu, D.V., Feurdean, A., Niedermeyer, E.M., Mulch., A., 2021. Severe late Miocene droughts affected Eurasia. Glob. Planet. Change. https://doi.org/10.1016/j.gloplacha.2021.103644.

Clark, P.U., Archer, D., Pollard, D., Blum, J.D., Rial, J.A., Brovkin, V., Mix, A.C., Pisias, N. G., Roy, M., 2006. The middle Pleistocene transition: characteristics, mechanisms, and implications for long-term changes in atmospheric pCO_2. Quat. Sci. Rev. 25, 3150–3184.

De Jonge, C., Hopmans, E.C., Zell, C.I., Kim, J.-H., Schouten, S., Sinninghe Damsté, J.S., 2014. Occurrence and abundance of 6-methyl branched glycerol dialkyl glycerol tetraethers in soils: Implications for palaeoclimate reconstruction. Geochim. Cosmochim. Acta 141, 97–112.

Doukas, C., van Kolfschoten, T., Papayianni, K., Panagopoulou, E., Harvati, K., 2018. The Small Mammal Fauna from the Palaeolithic Site Marathousa 1 (Greece). Quat. Int. 497, 95–107. https://doi.org/10.1016/j.quaint.2018.09.036.

Duncan, B., McKay, R., Bendle, J., Naish, T., Inglis, G.N., Moossen, H., Levy, R., Ventura, G.T., Lewis, A., Chamberlain, B., Walker, C., 2019. Lipid biomarker distributions in Oligocene and Miocene sediments from the Ross Sea region, Antarctica: implications for use of biomarker proxies in glacially-influenced settings. Palaeogeogr. Palaeoclimatol. Palaeoecol. 516, 71–89. https://doi.org/10.1016/j.palaeo.2018.11.028.

Eglinton, T.I., Eglinton, G., 2008. Molecular proxies for paleoclimatology. Earth Planet. Sci. Lett. 275 (1–2), 1–16. https://doi.org/10.1016/j.epsl.2008.07.012.

Eglinton, G., Hamilton, R.J., 1967. Leaf Epicuticular Waxes. Science (80-.) 156, 1322–1335 at: http://science.sciencemag.org/content/sci/156/3780/1322.full.pdf.

Falguères, C., Bahain, J.-J., Bischoff, J.L., Pérez-González, A., Ortega, A.I., Ollé, A., Quiles, A., Ghaleb, B., Moreno, D., Dolo, J.-M., Shao, Q., Vallverdú, J., Carbonell, E., Bermúdez de Castro, J.M., Arsuaga, J.L., 2013. Combined ESR/U-series chronology of acheulian hominid-bearing layers at trinchera Galería site, Atapuerca, Spain. J. Hum. Evol. 65, 168e184. https://doi.org/10.1016/j.jhevol.2013.05.005.

Feakins, S.J., Sessions, A.L., 2010. Controls on the D/H ratios of plant leaf waxes in an arid ecosystem. Geochim. Cosmochim. Acta 74, 2128–2141. https://doi.org/10.1016/j.gca.2010.01.016.

Ficken, K.J., Li, B., Swain, D.L., Eglinton, G., 2000. An *n*-alkane proxy for the sedimentary input of submerged/floating freshwater aquatic macrophytes. Org. Geochem. 31, 745–749.

Field, M.H., Ntinou, M., Tsartsidou, G., van Bergehenegowuen, D., Tourloukis, V., Thompson, N., Karkanas, P., Panagopoulou, E., Harvati, K., 2018. A palaeoenvironmental reconstruction (based on palaeobotanical data and diatoms) of the Middle Pleistocene elephant (*Palaeoloxodon antiquus*) butchery site at Marathousa, Megalopolis, Greece. Quat. Int. 497, 108–122.

Flanagan, L.B., Comstock, J.P., Ehleringer, J.R., 1991. Comparison of modelled and observed environmental influences on the stable oxygen and hydrogen isotope composition of leaf water in *Phaseolus vulgaris* L. Plant Physiol. 96, 588–596.

Gagosian, R.B., Peltzer, E.T., 1986. The importance of atmospheric input of terrestrial organic material to deep sea sediments. Org. Geochem. 10, 661–669. https://doi.org/10.1016/S0146-6380(86)80002-X.

Gaviria-Lugo, N., Läuchli, C., Wittmann, H., Bernhardt, A., Frings, P., Mohtadi, M., Rach, O., Sachse, D., 2023. Climatic controls on leaf wax hydrogen isotope ratios in terrestrial and marine sediments along a hyperarid-to-humid gradient. Biogeosciences 20, 4433–4453. https://doi.org/10.5194/bg-20-4433-2023.

Giusti, D., Tourloukis, V., Konidaris, G., Thompson, N., Karkanas, P., Panagopoulou, E., et al., 2018. Beyond Maps: patterns of Formation Processes at the Middle Pleistocene Open-Air Site of Marathousa 1, Megalopolis Basin, Greece. Quat. Int. 497, 137–153. https://doi.org/10.1016/j.quaint.2018.01.041.

Guibert-Cardin, J., Tourloukis, V., Thomson, N., Panagopoulou, E., Harvati, K., Nicoud, E., Beyries, S., 2022. The function of small tools in Europe during the Middle Pleistocene: the case of Marathousa 1 (Megalopolis, Greece). J. Lit. Stud. 9 (1), 29. https://doi.org/10.2218/jls.5553.

Harvati, K., Konidaris, G., Tourloukis, V. (Eds.), 2018. Special Issue Human Evolution at the Gates of Europe, 497 Part A. Quaternary International Special Issue, pp. 1–240.

Herrera-Herrera, A.V., Leierer, L., Jambrina-Enríquez, M., Connolly, R., Mallol, C., 2020. Evaluating different methods for calculating the Carbon Preference Index (CPI): Implications for palaeoecological and archaeological research. Org. Geochem. 146 https://doi.org/10.1016/j.orggeochem.2020.104056.

Hopmans, E.C., Weijers, J.W.H., Schefuss, E., Herfort, L., Sinninghe Damsté, J.S., Schouten, S., 2004. A novel proxy for terrestrial organic matter in sediments based on branched and isoprenoid tetraether lipids. Earth Planet. Sci. Lett. 224, 107–116. https://doi.org/10.1016/j.epsl.2004.05.012.

Hughes, P.D., Woodward, J.C., Gibbard, P.L., Macklin, M.G., Gilmour, M.A., Smith, G.R., 2006. The Glacial history of the Pindus Mountains, Greece. J. Geol. 114, 413–434.

Hughes, P.D., Woodward, J.C., Gibbad, P.L., 2007. Middle Pleistocene Cold Stage Climates in the Mediterranean: New evidence from the Glacial Record. Earth Planet. Sci. Lett. 253 (1–2), 50–56. https://doi.org/10.1016/j.epsl.2006.10.019.

Jacobs, Z., Li, B., Karkanas, P., Tourloukis, V., Thompson, N., Panagopoulou, E., Harvati, K., 2018. Optical dating of K-feldspar grains from Middle Pleistocene lacustrine sediment at Marathousa 1 (Greece). Quat. Int. 497, 170–177. https://doi.org/10.1016/j.quaint.2018.06.029.

Joannin, S., Bassinot, F., Combourieu Nebout, N., Peyron, O., Beudouin, C., 2011. Vegetation response to obliquity and precession forcing during the Mid-Pleistocene transition in Western Mediterranean region (ODP site 976). Quat. Sci. Rev. 30 (3–4), 280–297. https://doi.org/10.1016/j.quascirev.2010.11.009.

Jouzel, J., Masson-Delmotte, V., Cattani, O., Dreyfus, G., Falourd, S., Hoffman, G., Minster, B., Nouet, J., Barnola, J.M., Chappellaz, J., Fischer, H., Gallet, J.C., Johnsen, S., Leuenberger, D., Loulergue, L., Luethi, D., Oerter, H., Parrenin, F., Raisbeck, G.M., Raynaud, D., Schilt, A., Schwander, J., Selmo, E., Souchez, R.A., Spahni, R., Stauffer, B., Steffensen, J.P., Stenni, B., Stocker, T.F., Tison, J.L., Werner, M., Wolff, E.W., 2007. Orbital and Millennial Antarctic climate Variability over the past 800 000 years. Science 317, 793–796.

Karkanas, P., Tourloukis, V., Thompson, N., Giusti, D., Panagopoulou, E., Harvati, K., 2018. Sedimentology and micromorphology of the lower Palaeolithic lakeshore site Marathousa 1, Megalopolis basin, Greece. Quat. Int. 497, 123–136. https://doi.org/10.1016/j.quaint.2018.02.037.

Karkanas, P., Tourloukis, V., Thompson, N., Giusti, D., Tsartsidou, G., Athanassiou, A., Konidaris, G.E., Roditi, E., Panagopoulou, E., Harvati, K., 2024. The Megalopolis Paleoenvironmental Project (MegaPal). In: Katerina, Harvati, Melania, Ioannidouu (Eds.), Tuebingen Paleoanthropology Book Series-Contributions in Paleoanthropology, 03. Human Evolution at the Crossroads, Tübingen University Press.

Konidaris, G.E., Athanassiou, A., Tourloukis, V., Thompson, N., Giusti, D., Panagopoulou, E., Harvati, K., 2018. The Skeleton of a Straight-Tusked Elephant (Palaeoloxodon antiquus) and other large Mammals from the Middle Pleistocene Butchering Locality Marathousa 1 (Megalopolis Basin, Greece): preliminary results. Quat. Int. 497, 65–84. https://doi.org/10.1016/j.quaint.2017.12.001.

Konidaris, G.E., Athanassiou, A., Panagopoulou, E., Harvati, K., 2022. First record of Macaca (Cercopithecidae, Primates) in the Middle Pleistocene of Greece. J. Hum. Evol. 162, 103104 https://doi.org/10.1016/j.jhevol.2021.103104.

Köppen, W., 1918. Klassification der Klimate Nach Temperatur. Niederschlag and Jahreslauf. Petermanns Geographische Mitteilungen, p. 64.

Koutsodendris, A., Kousis, I., Peyron, O., Wagner, B., Pross, J., 2019. The Marine Isotope Stage 12 pollen record from Lake Ohrid (SE Europe): investigating short-term climate change under extreme glacial conditions. Quat. Sci. Rev. 221, 105873 https://doi.org/10.1016/j.quascirev.2019.105873.

Kroon, D., Alexander, I., Little, M., Lourens, L.J., Matthewson, A.H.F., Sakamoto, T., 1998. Oxygen isotope and sapropel stratigraphy in the Eastern Mediterranean during the last 3.2 million years. In: Proceedings of the Ocean Drilling Program, Scientific Results. Ocean Drilling Program, College Station, TX, pp. 181–189, 160.

Kutzbach, J.E., Chen, G., Cheng, H., Edwards, R.L., Liu, Z., 2014. Potential Role of winter Rainfall in explaining increased Moisture in the Mediterranean and Middle East during periods of Maximum Orbitally-Forced Insolation Seasonality. Clim. Dyn. 42 (3–4), 1079–1095. https://doi.org/10.1007/s00382-013-1692-1.

Laskar, J., Robutel, P., Joutel, F., Gastineau, M., Correia, A.C.M., Levrard, B., 2004. A long-term numerical solution for the insolation quantities of the Earth. Astron. Astrophys. 438 (1), 261–285. https://doi.org/10.1051/0004-6361:20041335.

Leontaritis, A.D., Kouli, K., Pavlopoulos, K., 2020. The Glacial history of Greece: a Comprehensive Review. Med. Geosc. Rev. 2 (2), 65–90. https://doi.org/10.1007/s42990-020-00021-w.

Lisiecki, L.E., Raymo, M.E., 2005. A Pliocene-Pleistocene Stack of 57 Globally distributed Benthic $\delta^{18}O$ Records. Paleoceanography 20. https://doi.org/10.1029/2004PA001071 a–n.

Liu, W.G., Yang, H., Li, L., 2006. Hydrogen isotopic compositions of *n*-alkanes from terrestrial plants correlate with their ecological life forms. Oecologia 150, 330–338.

Lourens, J.L., 2004. Revised tuning of Ocean Drilling Program Site 964 and KC01B (Mediterranean) and implications for the delta O-18, tephra, calcareous nannofossil, and geomagnetic reversal chronologies of the past 1.1 Myr. Paleoceanography 19, PA3010. https://doi.org/10.1029/2003PA000997.

Lüning, S., Schulte, L., Garcés-Pastor, S., Danladi, I.B., Gałka, M., 2019. The medieval climate Anomaly in the Mediterranean Region. Paleoceanogr. Paleoclimatol. 34, 1625–1649. https://doi.org/10.1029/2019PA003734.

Lüthi, D., Le Floch, M., Bereiter, B., Blunier, T., Barnola, J.M., Siegenthaler, U., Raynaud, D., Jouzel, J., Fischer, H., Kawamura, K., Stocker, T.F., 2008. High-resolution carbon dioxide concentration record 650 000–800 000 years before present. Nature 453, 379–382.

Mann, M.E., Zhang, Z., Rutherford, S., Bradley, R.S., Hughes, M.K., Shindell, D., et al., 2009. Global signatures and dynamical origins of the Little Ice Age and medieval climate Anomaly. Science 326 (5957), 1256–1260.

Martínez-Dios, A., Pelejero, C., Cobacho, S., Movilla, J., Dinarès-Turell, J., Calvo, E., 2021. A 1-million year record of environmental change in the Central Mediterranean Sea from organic molecular proxies. Paleoceanogr. Paleoclimatol. 36 https://doi.org/10.1029/2021PA004289 e2021PA004289.

Martínez-Sosa, P., Tierney, J.E., Ştefănescu, I., Dearing Crampton-Flood, E., Shuman, B. N., Routson, C., 2021. A global Bayesian temperature calibration for lacustrine brGDGTs. Geochim. Cosmochim. Acta 305, 87–105. https://doi.org/10.1016/j.gca.2021.04.038.

Marzi, R., Torkelson, B.E., Olson, R.K., 1993. A revised carbon preference index. Org. Geochem. 20, 1303–1306. https://doi.org/10.1016/0146-6380(93)90016-5.

Michailidis, D., Konidaris, G.E., Athanassiou, A., Panagopoulou, E., Harvati, K., 2018. The ornithological remains from Marathousa 1 (Middle Pleistocene; Megalopolis Basin, Greece). Quat. Int. 497, 85–94.

Müller, P.J., Kirst, G., Ruhland, G., von Storch, I., Rosell-Melé, A., 1998. Calibration of the alkenone paleotemperature index based on core-tops from the eastern South Atlantic and the global ocean (60°N–60°S). Geochim. Cosmochim. Acta 62 (10), 1757–1772. https://doi.org/10.1016/S0016-7037(98)00097-0.

Okuda, M., van Vugt, N., Nakagawa, T., Ikeya, M., Hayashida, A., Yasuda, Y., Setoguchi, T., 2002. Palynological evidence for the astronomical origin of lignite-detritus sequence in the middle Pleistocene Marathousa member, Megalopolis, SW Greece. Earth Planet. Sci. Lett. 201, 143–157. https://doi.org/10.1016/0025-326X(92)90532-B.

Panagopoulou, E., Tourloukis, V., Thompson, N., Konidaris, G., Athanassiou, A., Giusti, D., et al., 2018. The lower Palaeolithic Site of Marathousa 1, Megalopolis, Greece: Overview of the evidence. Quat. Int. 497, 33–46. https://doi.org/10.1016/j.quaint.2018.06.031.

Pearson, E.J., Juggins, S., Talbot, H.M., Weckström, J., Rosén, P., Ryves, D.B., Roberts, S. J., Schmidt, R., 2011. A lacustrine GDGT-temperature calibration from the

Scandinavian Arctic to Antarctic: renewed potential for the application of GDGT-paleothermometry in lakes. Geochim. Cosmochim. Acta 75, 6225–6238.
Pendoley, K., 1992. Hydrocarbons in Rowley Shelf (Western Australia) oysters and sediments. Mar. Pollut. Bull. 24 (4), 210–215.
Poli, M.S., Thunell, R.C., Rio, D., 2000. Millennial-scale changes in North Atlantic deep-water circulation during marine isotope stages 11 and 12: linkage to Antarctic climate. Geology 28 (9), 807e810.
Raberg, J.H., Harning, D.J., Crump, S.E., de Wet, G., Blumm, A., Kopf, S., Geirsdóttir, Á., Miller, G.H., Sepúlveda, J., 2021. Revised fractional abundances and warm-season temperatures substantially improve brGDGT calibrations in lake sediments. Biogeosciences 18 (12), 3579–3603. https://doi.org/10.5194/bg-18-3579-2021.
Ramos-Román, M.J., De Jonge, C., Magyari, E., Veres, D., Ilvonen, L., Develle, A.-L., Seppä, H., 2022. Lipid biomarker (brGDGT)- and pollen-based reconstruction of temperature change during the Middle to Late Holocene transition in the Carpathians. Glob. Planet. Change 215 (103859). https://doi.org/10.1016/j.gloplacha.2022.103859.
Raymo, M.E., Oppo, D., Curry, W., 2007. The mid-Pleistocene climate transition: a deep sea carbon isotope perspective. Paleoceanography 12, 546–559.
Regattieri, E., Giaccio, B., Galli, P., Nomade, S., Peronace, E., Messina, P., Sposato, A., Boschi, C., Gemelli, M., 2016. A multi-proxy record of MIS 11-12 deglaciation and glacial MIS 12 instability from the Sulmona basin (Central Italy). Quat. Sci. Rev. 132, 129e145. https://doi.org/10.1016/j.quascirev.2015.11.015.
Roditi, E., Bocherens, H., Konidaris, G.E., Athanassiou, A., Tourloukis, V., Karkanas, P., Panagopoulou, E., Harvati, K., 2024. Life-history of *Palaeoloxodon antiquus* reveals Middle Pleistocene glacial refugium in the Megalopolis basin, Greece. Sci. Report. 14, 1390. https://doi.org/10.1038/s41598-024-51592-9.
Sachse, D., et al., 2012. Molecular palaeohydrology: Interpreting the hydrogen-isotope biomarkers from photosynthesizing organisms. Ann. Rev. Earth Planet. Sci. 40, 221–249.
Schwark, L., Zink, K., Lechterbeck, J., 2002. Reconstruction of postglacial to early Holocene vegetation history in terrestrial Central Europe via cuticular lipid biomarkers and pollen records from lake sediments. Geology 30 (5), 463–466. https://doi.org/10.1130/0091-7613(2002)030<0463:ROPTEH>2.0.CO;22002;30;463-466.
Sinninghe Damsté, J.S., Hopmans, E.C., Pancost, R.D., Schouten, S., Geenevasen, J.A.J., 2000. Newly discovered non-isoprenoid dialkyl diglycerol tetraether lipids in sediments. J. Chem. Soc. Chem. Commun. 23, 1683–1684.
Sinninghe Damsté, J.S., Rijpstra, W.I.C., Foesel, B.U., Huber, K.J., Overmann, J., Nakagawa, S., Kim, J.J., Dunfield, P.F., Dedysh, S.N., Villanueva, L., 2018. An overview of the occurrence of ether-and ester-linked iso-diabolic acid membrane lipids in microbial cultures of the Acidobacteria: Implications for brGDGT paleoproxies for temperature and pH. Org. Geochem. 124, 63–76.
Tourloukis, V., Thomson, N., Panagopoulou, E., Giusti, D., Konidaris, G.E., Karkanas, P., Harvati, K., 2018a. Lithic artifacts and bone tools from the lower Palaeolithic site Marathousa 1, Megalopolis, Greece: preliminary results. Quat. Int. 497, 47–64. https://doi.org/10.1016/j.quaint.2018.05.043.
Sun, Q., Chu, G., Liu, M., Xie, M., Li, S., Ling, Y., Wang, X., Shi, L., Jia, G., Lü, H., 2011. Distributions and temperature dependence of branched glycerol dialkyl glycerol tetraethers in recent lacustrine sediments from China and Nepal. J. Geophys. Res. Biogeosci. 116 https://doi.org/10.1029/2010jg001365.
Tourloukis, V., Muttoni, G., Karkanas, P., Monesi, E., Scardia, G., Panagopoulou, E., Harvati, K., 2018b. Magnetostratigraphic and chronostratigraphic constraints on the Marathousa 1 lower Palaeolithic site and the middle Pleistocene deposits of the Megalopolis basin, Greece. Quat. Int. 497, 154–169. https://doi.org/10.1016/j.quaint.2018.03.043.
Trauth, M.H., 2014. A new probabilistic technique to build an age model for complex stratigraphic sequences. Quat. Geochronol. 22, 65–71. https://doi.org/10.1016/j.quageo.2014.03.001.
Tzedakis, P.C., Hooghiemstra, H., Pälike, H., 2006. The last 1.35 Million Years at Tenaghi Philippon: revised Chronostratigraphy and Long-Term Vegetation Trends. Quat. Sci. Rev. 25 (23–24), 3416–3430. https://doi.org/10.1016/j.quascirev.2006.09.002.
van de Wal, R.S.W., de Boer, B., Lourens, L.J., Köhler, P., Bintanja, R., 2011. Reconstruction of a continuous high-resolution CO2 record over the past 20 million years. Clim. Past 7, 1459–1469. https://doi.org/10.5194/cp-7-1459-2011.
Vidal, L., Labeyrie, L., Cortijo, E., Arnold, M., Duplessy, J.C., Michel, E., Van Weering, T.C.E., 1997. Evidence for changes in the North Atlantic deep water linked to meltwater surges during the Heinrich events. Earth Planet. Sci. Lett. 146 (1), 13e27.
Villa, V., Pereira, A., Chaussé, C., Nomade, S., Giaccio, B., Limondin-Lozouet, N., Fusco, F., Regattieri, E., Degeai, J.-P., Robert, V., Kuzucuoglu, C., Boschian, G., Agostini, S., Aureli, D., Pagli, M., Bahain, J.J., Nicoud, E., 2016. A MIS 15-MIS 12 record of environmental changes and lower Palaeolithic occupation from Valle Giumentina, Central Italy. Quat. Sci. Rev. 151, 160–184. https://doi.org/10.1016/j.quascirev.2016.09.006.
Vinken, R., 1965. Stratigraphie und Tektonik des Beckens von Megalopolis (Peloponnes, Griechenland). Geol. Jahrb. 83, 97–148.
Weijers, J.W.H., Schouten, S., van der Donker, J., Hopmans, E.C., Sinninghe Damsté, J., 2007. Environmental controls on bacterial tetraether membrane lipid distribution in soils. Geochim. Cosmochim. Acta 71, 703–713.
Weiss, G.M., Schouten, S., Lattaud, J., van der Meer, M.T.J., Eglinton, T.I., 2022. Co-evolution of the terrestrial and aquatic ecosystem in the Holocene Baltic Sea. Clim. Past 18 (2), 233–248. https://doi.org/10.5194/cp-18-233-2022.
Zachos, J.C., Dickens, G.R., Zeebe, R.E., 2008. An early Cenozoic perspective on greenhouse warming and carbon-cycle dynamics. Nature 451 (7176), 279–283. https://doi.org/10.1038/nature06588.